Entropic Nature of the Interaction between Promoter Bound CRP Mutants and RNA Polymerase†

Susan Krueger,‡ Susan Gregurick,§ Ying Shi,|| Shenglun Wang,|| Brian D. Wladkowski,⊥ and Frederick P. Schwarz*,||

National Institute of Science and Technology Center for Neutron Research, Gaithersburg, Maryland 20899, Department of Chemistry and Biochemistry, University of Maryland, Baltimore County, 1000 Hilltop Circle, Baltimore, Maryland 21250, Center for Advanced Research in Biotechnology/National Institute of Science and Technology, 9600 Gudelsky Drive, Rockville, Maryland 20850, and Department of Chemistry, Western Maryland College, 2 College Hill, Westminister, Maryland 21157

Received August 29, 2002; Revised Manuscript Received December 20, 2002

ABSTRACT: The interaction between CRP, T127L, S128A, and CRP* and RNA polymerase bound to a 104 bp synthetic promoter were determined by ITC at 298 K and ranges from a $\Delta G_b^\circ = 1.4 \pm 0.8$ kJ mol^{-1} (cAMP-ligated S128A) to 4.5 ± 0.3 kJ mol^{-1} (cAMP-ligated double mutant CRP*) with endothermicities that range from 4 ± 3 kJ mol^{-1} (cAMP-ligated CRP) to 47 ± 8 kJ mol^{-1} (cGMP-ligated T127L). The interaction is, thus, entropically driven, exhibits enthalpy−entropy compensation, and increases the binding affinity of the RNA polymerase to the promoter by factors ranging from 1.7 ± 0.1 (cAMP-ligated S128A) to 6.1 ± 0.1 (cAMP-ligated CRP*). Although the binding affinities to the promoter alone, except for cAMP-ligated S128A, are the same as to a shorter 40 bp duplex containing the same CRP consensus binding site sequence (conDNA), the binding enthalpies of CRP/mutant to the promoter are lower by factors of 2−3× than the corresponding binding enthalpies to conDNA. Small angle neutron scattering measurements on the DNA−CRP/mutant complexes in D_2O/H_2O solutions exhibit an increase in the *R*g of the CRP/mutant component from 22 to 27−31 Å that can be attributed to a conformational change in the N-terminal domain of CRP. The *R*g = 27 Å for the bound conDNA can be attributed to a slight unwinding of the DNA in solution that would also enhance the activation of transcription. The *R*g $= 53 \pm 3$ Å for the bound promoter is attributed to bending of the promoter in solution that can be responsible for the lower CRP/mutant−promoter binding endothermicities.

The transcription of enzymes that metabolize carbohydrates in *Escherichia coli* is enhanced by the binding of cAMP receptor protein (CRP)[1] to a site on the promoter that is centered at −61.5 bp upstream from the transcription start point and adjacent to the RNA polymerase binding site. This enhancement can been attributed to (i) an increase in the binding affinity of RNA polymerase to the promoter by CRP (*1*, *2*), (ii) bending of the promoter by CRP resulting in more contacts between the RNA polymerase and the promoter (*3*), and/or (iii) an increase in the conversion rate of the RNA polymerase−promoter complex from a closed form to the transcriptionally active open form by CRP (*2*). CRP is a 47 000 g mol^{-1} dimer with the C-terminal domain of each subunit binding to the promoter site upon activation of the protein by binding of cAMP to the N-terminal domain. The cAMP-ligated CRP binding affinity to the promoter sequence can be altered by mutations at the CRP subunit interface such as the T127→L mutation (T127L), the S128→A mutation (S128A), double mutations consisting of T127→L and S128→A (CRP*), and by cGMP instead of cAMP ligated to the T127L and CRP* mutants (*4*). Although the binding affinities of the mutants to a 104 bp synthetic promoter containing the CRP consensus binding sequence (*syncon* promoter) range from $1.1 \pm 0.1 \times 10^6$ M^{-1} (cAMP-ligated CRP*) to $6.6 \pm 1.1 \times 10^6$ M^{-1} (cAMP-ligated CRP) (*4*), the binding affinities of the CRP mutants to the RNA polymerase−promoter complex vary only from 0.80 ± 0.20 to $2.2 \pm 1.2 \times 10^7$ M^{-1} (*5*). This is in closer agreement with the observed variation from 11.7 ± 0.5 to 13 ± 1 in the enhancement of in vitro transcription by the CRP mutants (*5*). A weaker binding affinity of a CRP mutant to the promoter is apparently compensated by a stronger binding interaction between the CRP mutant and the bound RNA polymerase. Undoubtedly, CRP increases the binding affinity of RNA polymerase to the promoter by providing additional indirect interactions between the RNA polymerase and through the CRP to the promoter. However, the nature of the interaction between the CRP mutant and the bound RNA

† This work was supported by National Science Foundation Grant MCB-9722884 to F.P.S., National Science Foundation Grant 9983321 to B.D.W., and National Science Foundation Grant DMR-9423101 to the Center for High-Resolution Neutron Scattering at National Institute of Science and Technology.

* Corresponding author. E-mail: fred@carb.nist.gov.

‡ National Institute of Science and Technology Center for Neutron Research.

§ University of Maryland.

|| Center for Advanced Research in Biotechnology/National Institute of Science and Technology.

⊥ Western Maryland College.

[1] Abbreviations: cAMP, 3′-5′ cyclic adenosine monophosphate; cGMP, 3′-5′ cyclic guanosine monophosphate; CRP, cAMP receptor protein; CRP*, T127→L/S128→A CRP mutant; ITC, isothermal titration calorimetry; *R*g(Complex), radius of gyration of the CRP−DNA complex; *R*g(CRP), radius of gyration of the CRP component of the complex; *R*g(DNA), radius of gyration of the DNA component of the complex; SANS, small angle neutron scattering; T127L, T127→L CRP mutant; S128A, S128→A CRP mutant.

10.1021/bi026755v CCC: $25.00
Published on Web 01/30/2003

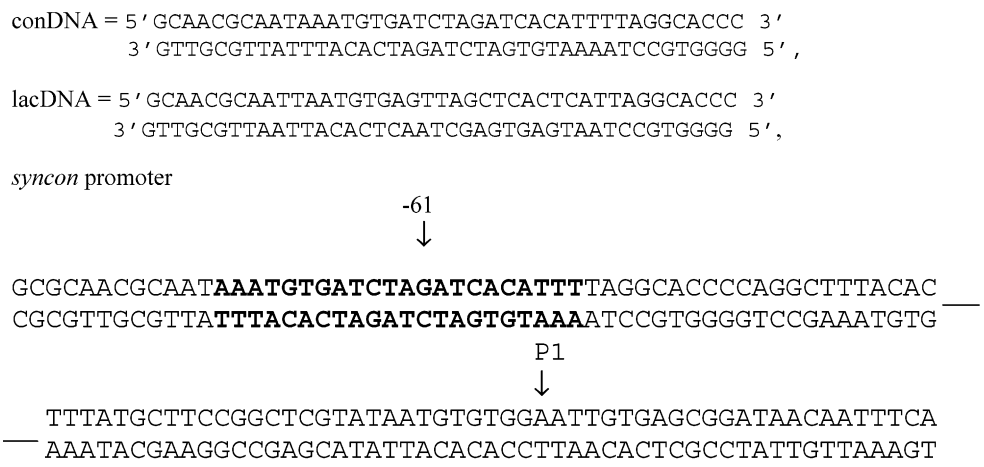

FIGURE 1: Sequences for the conDNA, lacDNA, and *syncon* promoter. In the *syncon* promoter, the CRP consensus binding site is in bold letters, and P1 is the transcription start point.

polymerase still remains to be determined.

The bending of the promoter by CRP to increase interactions between the RNA polymerase and the promoter was inferred from early X-ray crystal structures of the cAMP-ligated CRP−short DNA complexes that showed the bound DNA to be bent by 90° (*6*). In addition to bending of the promoter, conformational changes in the CRP may also occur upon binding to the promoter to facilitate interactions with the adjacently bound RNA polymerase. This is based on the premise that the interaction between CRP and bound RNA polymerase is analogous to the interactions between transcription factors and an RNA polymerase in the preinitiation transcription complex in eukaryotic transcription. Proteolysis probes (*7*), circular dichroism measurements (*7*−*9*), fluorescence measurements (*8*), and NMR measurements (*9*) show that these transcription factors undergo local and global folding processes in their DNA-binding domains upon binding to the promoter. These conformational changes, such as in the transcription factor Ets-1 (*7*), can provide additional contact points with other proteins in preinitiation complex to activate transcription in eukaryotes. Protein footprinting analysis of the cAMP-ligated CRP complex in solution do indeed imply that CRP undergoes an additional conformational change in the N-terminal domains upon binding to ≥30 bp DNA duplexes containing the CRP consensus binding-site sequence (*10*). However, since this conformational difference in the N-terminal domain is not observed in a comparison between the crystal structures of the DNA-bound and unbound cAMP-ligated CRP complexes (*6*, *11*−*13*), it may be minimized by crystal-packing forces in the crystallization of the protein complexes. Furthermore, the 30 bp DNA in the crystal structure consisted of two overlapping DNA fragments in contrast to the >30 bp DNA duplexes used in the solution studies (*4*, *10*). It is, thus, necessary to determine if bending of the promoter analogous to the bent DNA in the X-ray crystal structure of cAMP-ligated CRP−DNA complexes as well as conformational changes in the CRP upon promoter binding does occur in solution to provide a more complete understanding of how the activation of transcription is enhanced by CRP.

In this investigation, the enthalpy and entropy changes that determine the binding affinities of the CRP mutants to the *syncon* promoter (Figure 1) were determined by isothermal titration calorimetry (ITC) measurements and compared to the corresponding changes that determine the binding affinities of the CRP mutants to an RNA polymerase−promoter complex. The promoter consists of a 104 bp section from −82 to 22 of the *lacUV5* promoter that contains the RNA polymerase binding site and was modified to a consensus CRP binding sequence centered at −61 bp (*syncon* promoter). Differences between these thermodynamic parameters are then attributed to the interaction between the bound CRP mutant and the bound RNA polymerase. Since this interaction between the bound CRP mutant and the RNA polymerase may be facilitated by a conformational change in CRP upon binding to the promoter, small angle neutron scattering (SANS) measurements were employed to directly determine if any conformational change occurs in CRP upon binding to the promoter site, as mimicked by a shorter 40 bp CRP consensus duplex (conDNA) and a 40 bp duplex that contained the CRP binding sequence from the *lacUV5* promoter (lacDNA) (Figure 1). An increase in the radius of gyration of the CRP mutant from 22 to 30 Å in the promoter site-bound state is indeed observed in SANS measurements on the CRP/mutant−conDNA complex in solution. The SANS data are then compared to simulated SANS data from a distorted energy-minimized X-ray crystal structure of the protein component of the cAMP-ligated CRP−DNA complex to determine the nature of this conformational change. The DNA component was modeled as a bent rigid rod in these calculations and exhibited partial unwinding, characteristic of the active open form of the RNA polymerase−promoter transcription complex. Furthermore, SANS data on the 104 *syncon* promoter bound to the CRP/mutants show that it is in the bent conformation, which would facilitate contacts between the promoter and the RNA polymerase. Although there is general agreement between the CRP mutant binding affinities to the 104 bp *syncon* promoter and the shorter 40 bp conDNA duplex, the binding enthalpy change to the shorter sequence is larger than that to the longer sequence. This difference is explored in terms of the long-range electrostatic forces contributing to the binding enthalpy with the longer promoter.

EXPERIMENTAL PROCEDURES

Materials. The CRP and mutants were expressed, purified, and assayed according to the procedures described previously (*4*). The concentration of the CRP/mutants was determined

from UV measurements at 280 nm using an extinction coefficient of 3.5×10^4 M^{-1} cm^{-1} (*14*). The RNA polymerase holoenzyme was prepared and purified according to the procedure described by Lowe et al. (*15*), and an extinction coefficient of 2.77×10^5 cm^{-1} M^{-1} at 280 nm was used to determine the concentration of the RNA polymerase (*16*). The complementary 40 bp conDNA and lacDNA strands were obtained commercially at a purity level >90% as assayed by capillary electrophoresis and an analytical ion exchange column. Gel electrophoresis of the conDNA and lacDNA strands revealed essentially one intense band at 12 000 g, the molecular mass of the strand. The DNA duplexes were prepared by annealing complementary single DNA strands as described previously (*4*), and their concentrations were determined from UV absorption measurements using an extinction coefficient of 5.33×10^5 M^{-1} cm^{-1} (*17*). The 104 bp *syncon* promoter was from −82 to +22 of the *lacUV5* promoter, so that it contained the CRP and RNA polymerase binding site sequences shown in Figure 1. Each complementary strand of the 104 bp promoter was synthesized on the μmol level on a DNA synthesizer and purified by gel electrophoresis. The complementary sequences were annealed by heating equal amounts of each strand in 10 mM Tris/HCl buffer containing 1 mM $MgCl_2$ and 0.5 M NaCl at pH = 7.4 up to 95 °C followed by slow cooling to room temperature. The concentration of the 104 bp *syncon* promoter was determined from OD measurements at 260 nm using an extinction coefficient of 1.3×10^6 cm^{-1} M^{-1} based on an OD of 1 for a 50 ng μL^{-1} solution (*18*) and a molecular mass of 65 000 g mol^{-1}.

The phosphate buffer solution was 50 mM K_3PO_4 and contained 0.2 mM DTT, 0.2 mM EDTA, and 0.15 mM KCl at pH = 7.0. For the cAMP-ligated and cGMP-ligated CRP/mutant titrations, the buffer contained 1 mM of the cyclic nucleotide monophosphate to ensure that the CRP/mutant was all complexed with the ligand. The potassium phosphate salts, NaCl, KCl, Tris, $MgCl_2$, sodium salts of cAMP and cGMP, mercaptoethanol, polyacrylamide, bromophenol blue, and urea were reagent grade from Sigma Chemical Co.[2] The DTT was ultrapure brand from GIBCOBRL. The sodium salt of EDTA was from Serva Co. The HCl and glycerol were reagent grade from Mallinckrodt.

ITC Measurements. The binding affinity, enthalpy, and entropy of the cNMP-ligated CRP/mutants to the 104 bp *syncon* promoter and the promoter−RNA polymerase complex were determined from ITC measurements, using a Microcal, Inc. VP Titration Calorimeter as described previously (*4*, *5*). The sample vessel contained either the RNA polymerase, the RNA polymerase−104 bp *syncon* promoter complex, or the promoter alone in the phosphate buffer, while the reference vessel contained just the buffer solution. First, 2−4 μL aliquots of the 0.03−0.1 mM promoter solution were titrated 3−4 min apart into the 1−3 μM RNA polymerase sample solution until the binding was saturated as evident by the lack of a heat exchange signal. After adding cNMP to the promoter−RNA polymerase solution, 10 μL aliquots of a 0.03−0.06 mM cNMP-ligated CRP/mutant solution were titrated into the promoter−RNA polymerase complex solution. In a separate titration, the cNMP-ligated CRP/mutant solution was titrated into the sample vessel containing just a 1−3 μM promoter solution. For each of the titrations, the additions were continued for 2−3 times past saturation so that a heat of dilution of the titrant could be determined from these additional peak areas. For the promoter into RNA polymerase titrations, these extra additions amounted to about a 7% excess of the promoter to RNA polymerase concentration. The heats of dilution obtained from titrating the ligand just into the buffer solution were then subtracted from the heats obtained during the titration prior to analysis of the data.

A nonlinear, least-squares minimization software program from Microcal, Inc., Origin 5.0 (*19*), was used to fit the incremental heat of the *i*th titration (ΔQ (*i*)) of the total heat, Q_t, to the total titrant concentration, X_t, according to the following equations:

$$Q_t = nC_t\Delta H_b^o V\{1 + X_t/nC_t + 1/nK_bC_t - [(1 + X_t/nC_t + 1/nK_bC_t)^2 - 4X_t/nC_t]^{1/2}\}/2 \quad (1a)$$

$$\Delta Q(i) = Q(i) + dVi/2V\{Q(i) + Q(i-1)\} - Q(i-1) \quad (1b)$$

where C_t is the total RNA polymerase−promoter complex or promoter concentration in the sample vessel, V is the volume of the sample vessel, and n is the stoichiometry of the binding reaction, to yield values of K_b, ΔH_b^o, and n.

SANS Measurements. The concentrations of the SANS solutions ranged from 0.01 to 0.09 mM of cAMP-ligated CRP, cAMP-ligated T127L, or CRP* and were complexed with the conDNA, lacDNA, or *syncon* promoter in the phosphate buffer. To confirm that the complexes had the 1:1 stoichiometry for DNA binding, the complexes were formed in an ITC by titrating the DNA into the protein solution until the binding reached saturation. For the cAMP-ligated complexes, the buffer contained 1 mM cAMP so that the protein in the SANS solution was saturated with bound cAMP. For the contrast variation technique, the solutions were dialyzed in the appropriate D_2O/H_2O buffer.

SANS measurements were performed on the CHRNS 30 m SANS instrument at the NIST Center for Neutron Research in Gaithersburg, MD (*20*). The neutron wavelength, λ, was 5 Å, with a wavelength spread, $\Delta\lambda/\lambda$, of 0.15. The neutron scattering intensity was corrected for background scattering from the buffers and incoherent scattering from hydrogen in the samples. Data were placed on an absolute scale by normalizing the scattering intensity to the incident beam flux. Finally, the data were radially averaged to produce scattering intensity, $I(Q)$, versus Q curves, where $Q = 4\pi \sin(\theta)/\lambda$, and 2θ is the scattering angle. The Guinier approximation, $I(Q) = I(0) \exp(-Q^2Rg^2/3)$, was used on the low-$Q$ portions of the data to obtain initial values for the radius of gyration, Rg, and the forward scattering intensity, $I(0)$, of the samples. This analysis is valid in the region $QRg \sim 1$. In the cases where higher Q data were available, the GNOM program (*21*) was used to determine the distance distribution function, $P(r)$, the radius of gyration, and the forward scattering intensity. The advantage of this approach is that all of the data are used, rather than a limited data set

[2] Certain commercial materials, instruments, and equipment are identified in this manuscript to specify the experimental procedure as completely as possible. In no case does such identification imply a recommendation or endorsement by the National Institute of Standards and Technology nor does it imply that the materials, instruments, or equipment identified is necessarily the best available for the purpose.

at small Q values, leading to more accurate determinations of Rg and $I(0)$ that are less influenced by possible aggregation effects.

The scattering intensities from the CRP−DNA complexes were decomposed into the scattering from their components, $I_{CRP}(Q)$ (or $I_{CRP}{}^*(Q)$) and $I_{DNA}(Q)$ using the following equation:

$$I(Q) = \Delta\rho_{CRP}{}^2 I_{CRP}(Q) + \Delta\rho_{CRP}\Delta\rho_{DNA} I_{CRPDNA}(Q) + \Delta\rho_{DNA}{}^2 I_{DNA}(Q) \quad (2)$$

where $\Delta\rho = (\rho - \rho_s)$ is the contrast, or the difference between the scattering length density of the molecule (ρ) and the solvent (ρ_s). The cross-term, $I_{CRPDNA}(Q)$, represents the interference function between the CRP and the DNA components. The known quantities in eq 2 are $\Delta\rho_{CRP}$ and $\Delta\rho_{DNA}$, and the unknowns are $I_{CRP}(Q)$, $I_{DNA}(Q)$, and $I_{CRPDNA}(Q)$. Since measurements were made at three different contrasts, or D_2O/H_2O buffer conditions, there is sufficient information to solve for the three unknown component intensities from the set of simultaneous equations for $I(Q)$ at each contrast.

Monte Carlo Simulations. Monte Carlo simulations of the SANS intensity from the CRP component of the complex were performed by representing each amino acid as a homogeneous sphere and calculating the size and neutron scattering strength of each sphere from the known volume and chemical composition of the amino acid. Once a sphere has been drawn around each amino acid, centered about the coordinates of its α-carbon atom, a box is drawn around the entire molecule with a region of bound water up to 5 Å thick. Points are generated at random within the box. The distance distribution function, $P(r)$, for the total volume is calculated in real space by making a histogram representing the distances between all possible pairs of points, weighted according to the product of the neutron scattering strengths at each point (*22*). A distorted energy-minimized X-ray crystal structure of a cAMP-ligated CRP−DNA complex was used for simulating the SANS intensities. The starting structure for the minimizations was the protein portion of the Protein Data Bank file 1BER by Parkinson et al. (*12*) with a distortion in the structure that consisted of relaxing the torsional angle between the C and the B α-helices. The addition of cAMP to the structure as described by Passner and Steitz (*13*) made very little difference in the simulations. Minimization of the starting structure employed the AMBER force field parameters and used the method of steepest descent.

The DNA structure was represented as a bent 10 Å diameter rod of uniform neutron scattering length density. The DNA portion of the Parkinson et al. (*12*) crystal structure was used as a guide to determine the position and structure of the bends in the DNA. The total length of the rod is dependent on the number of base pairs in the DNA, where each base pair is represented by a segment 3.4 Å in length. Thus, for the 40 bp lacDNA and conDNA the total rod length was 136 Å, and for the 104 bp *syncon* promoter the total rod length was 354 Å.

RESULTS

ITC Measurements. The results of ITC titrations of cAMP-ligated CRP solution into the 104 bp *syncon* promoter solution without bound RNA polymerase are shown in Figure 2 and with bound RNA polymerase in Figure 3. The results of these binding reactions are summarized in Table 1 for cAMP-ligated CRP, T127L, S128A, and CRP* and cGMP-ligated T127L. In the absence of bound RNA polymerase, the binding affinities to the *syncon* promoter range from $1.6 \pm 0.2 \times 10^6$ (cAMP-ligated CRP*) to $8.4 \pm 0.5 \times 10^6$ M^{-1} (cAMP-ligated S128A) and are consistently slightly higher but still, with the exception of the cAMP-ligated S128A mutant, within experimental error of the corresponding binding affinities to the 40 bp conDNA duplex containing just the 26 bp consensus sequence. It is not clear as to why the cAMP-ligated S128A binding affinity to the *syncon* promoter is 4−6× larger than to the conDNA duplex. The ligated CRP/mutant binding affinities to the promoter with RNA polymerase bound to the promoter are all higher, ranging from $9.8 \pm 0.1 \times 10^6$ (cAMP-ligated CRP*) to $16.1 \pm 4.6 \times 10^6$ M^{-1} (cAMP-ligated CRP), as observed earlier (*5*) and are attributed to additional interactions between the CRP and the RNA polymerase (*5*). Differences in the binding free energy, enthalpy, and entropy between the ligated CRP/mutant binding to the promoter with and without bound RNA polymerase are presented in Table 2. These differences are attributed to the interaction thermodynamic parameters between the bound RNA polymerase and the ligated CRP/mutant.

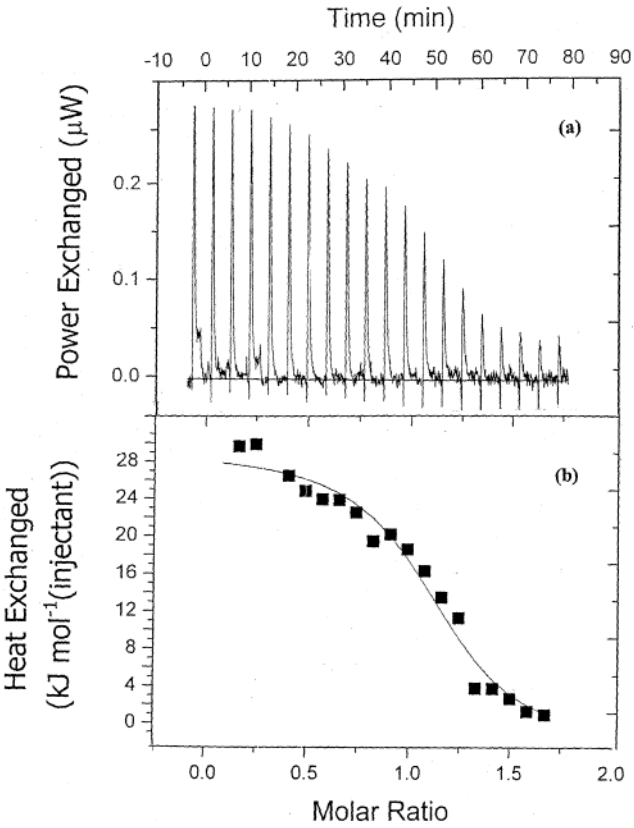

FIGURE 2: ITC titration of 5 μL aliquots of 0.060 mM cAMP-ligated CRP into 3.0 μM of 104 bp *syncon* promoter in the potassium phosphate + 1.0 mM cAMP buffer at pH = 7.0 and 298 K. The molar ratio is the ratio of the number of moles of cAMP-ligated CRP to the number of moles of the *syncon* promoter−RNA polymerase complex in the cell. (a) The binding isotherm for the titration in panel a where the solid line is the fit of the data to the binding model described by eq 1 (b).

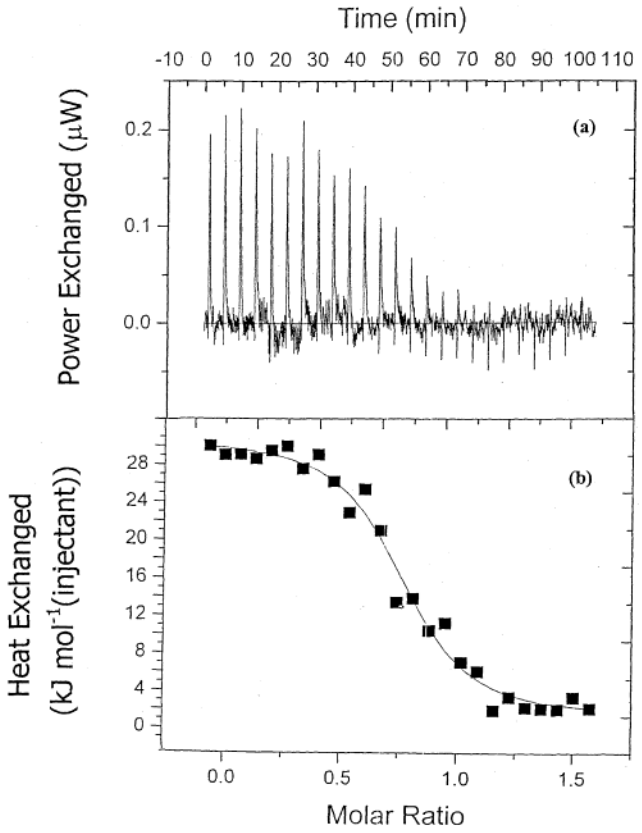

FIGURE 3: ITC titration of 5 μL aliquots of 0.060 mM cAMP-ligated CRP into 3.0 μM of 104 bp *syncon* promoter complexed with RNA polymerase in the potassium phosphate buffer + 1.0 mM cAMP buffer at pH = 7.0 and 298 K. The molar ratio is the ratio of the number of moles of cAMP-ligated CRP to the number of moles of the *syncon* promoter−RNA polymerase complex in the cell. (a) The binding isotherm for the titration in panel a where the solid line is the fit of the data to the binding model described by eq 1.

These differences show that the interaction between the cNMP-ligated CRP/mutant and the RNA polymerase on the promoter is solely driven by an increase in the entropy. These interaction enthalpies and entropies exhibit enthalpy−entropy compensation where a change in the binding enthalpy is compensated by a corresponding change in the entropy. Also, as observed earlier (*5*), a weak interaction between the promoter and the CRP/mutant is compensated by a strong interaction between the CRP/mutant and the RNA polymerase in the CRP/mutant−RNA polymerase−promoter complex. To determine how much the interaction between CRP/mutants and the RNA polymerase bound to the promoter enhances the binding affinity of the RNA polymerase to the promoter, the following binding reactions were combined:

$$\textit{syncon}\ \text{promoter} + \text{RNA polymerase} \Leftrightarrow \textit{syncon}\ \text{promoter}\cdot\text{RNA polymerase} \quad (3a)$$

$$\text{CRP} + \textit{syncon}\ \text{promoter}\cdot\text{RNA polymerase} \Leftrightarrow \text{CRP}\cdot\textit{syncon}\ \text{promoter}\cdot\text{RNA polymerase} \quad (3b)$$

$$\text{CRP} + \textit{syncon}\ \text{promoter} \Leftrightarrow \text{CRP}\cdot\textit{syncon}\ \text{promoter} \quad (3c)$$

to yield the following net reaction for binding of the RNA polymerase to the CRP·*syncon* promoter complex

$$\text{RNA polymerase} + \text{CRP}\cdot\textit{syncon}\ \text{promoter} \Leftrightarrow \text{RNA polymerase}\cdot\text{CRP}\cdot\textit{syncon}\ \text{promoter} \quad (4)$$

A comparison of the free energy change for this net reaction with that of RNA polymerase to the promoter alone from ref *5* shows that the binding affinity of RNA polymerase to the promoter site is enhanced by factors of 1.8 for cAMP-ligated S128A and to 6.1 for cAMP-ligated CRP* (Table 2) by the interaction between the CRP/mutant and the RNA polymerase.

Although the cNMP-ligated CRP/mutant binding affinities to conDNA and the *syncon* promoter are within experimental error, the binding enthalpies to the shorter 40 bp conDNA are 2−3× more endothermic than to the longer 104 bp *syncon* promoter. To determine if long-range electrostatic interactions on the longer promoter can account for this difference through additional exothermic contributions to the binding enthalpy, ITC titrations were performed on CRP and several mutants binding to the promoter at a higher ionic strength of 0.5 M KCl that would shield these long-range electrostatic interactions. The results at this higher ionic strength are compared to similar binding results to the conDNA at 0.5 M KCl from ref *4* in Table 3. Comparison of the results in Tables 1 and 3 show that the conDNA and the *syncon* promoter binding free energy changes are all lower at the higher ionic strength. Although values for ΔG_b° are in agreement for binding of conDNA and the *syncon* promoter at the higher ionic strength, the conDNA and *syncon* promoter binding enthalpies are the same only for cAMP-ligated CRP but different for cAMP-ligated T127L and for cAMP-ligated S128A. Since the differences between the conDNA and promoter binding enthalpies are maintained at the high salt concentration for two of the three complexes investigated, it is unlikely that long-range electrostatic interactions on the promoter can account for the differences in the cNMP-ligated CRP/mutant binding enthalpies to conDNA and to the *syncon* promoter.

SANS Measurements. SANS measurements on the cAMP-ligated CRP−conDNA complex in 0% D_2O buffer solution over a concentration range of 0.01−0.04 mM are presented in Figure 4, in the form of Guinier, or ln(I) versus Q^2, plots. Consistent values of Rg(Complex) were extracted from the slopes of the fitted curves in Figure 3, 28.8 ± 1.7 Å at 0.04 mM, 26.6 ± 0.6 Å at 0.02 mM, and 26.4 ± 0.8 Å at 0.01 mM, and thus, show that aggregation effects are absent in these solutions. Averages of Rg(Complex) values over all concentrations yield a value of 27.3 ± 0.8 Å for the CRP complex and 28.7 ± 0.6 Å for the CRP* complex as shown in Table 4. These values are larger than the Rg values of 21.6 ± 0.2 Å for CRP alone and 22.2 ± 0.2 Å for CRP* alone (*22*). Similar increases in Rg(Complex) that are independent of concentration were also observed for the cAMP-ligated CRP−lacDNA complex and are shown in Table 4. A similar value for Rg(Complex) was also observed for cAMP-ligated T127L−conDNA complex. The increase in Rg(Complex) could result from addition of the DNA component and/or from an increase in Rg(CRP) upon DNA binding. Table 4 also shows the values of Rg for the cAMP-ligated CRP/mutant−*syncon* promoter complexes. The Rg is considerably larger for the *syncon* promoter complexes, indicating that the addition of the DNA is clearly making some contribution to the increased Rg in this case, most likely because of the addition of the much larger DNA component.

To differentiate the neutron scattering intensity of the DNA component from that of the CRP, a contrast variation series

Table 1: Thermodynamic Quantities for cNMP-Ligated CRP Mutants Binding to Promoter in the Absence and Presence of RNAP Bound to the Promoter

promoter length	RNAP	−CRP mutant	cNMP	T (K)	$K_b \times 10^6$ (M^{-1})	$-\Delta G_b^\circ$ (kJ mol^{-1})	ΔH_b° (kJ mol^{-1})	ΔS_b° (J mol^{-1} K^{-1})
104 bp	+	CRP	cAMP	298	16.1 ± 4.6	41.1 ± 0.7	30 ± 2	239 ± 15
104 bp	−	CRP	cAMP	298	7.5 ± 1.1	39.2 ± 0.4	27 ± 3	222 ± 10
40 bp[a]	−	CRP	cAMP	296	6.6 ± 1.1	38.6 ± 0.4	84 ± 4	416 ± 17
104 bp	+	T127L	cAMP	298	15.8 ± 3.9	41.1 ± 0.6	56.7 ± 0.2	328 ± 2
104 bp	−	T127L	cAMP	298	5.1 ± 0.8	38.3 ± 0.4	61.1 ± 0.7	334 ± 3
40 bp[a]	−	T127L	cAMP	296	3.4 ± 0.5	37.0 ± 0.4	129 ± 9	564 ± 30
104 bp	+	T127L	cGMP	298	10.2 ± 1.8	40.0 ± 0.4	127 ± 8	426 ± 27
104 bp	−	T127L	cGMP	298	2.7 ± 0.3	36.7 ± 0.3	80 ± 1	389 ± 4
40 bp[a]	−	T127L	cGMP	297	2.3 ± 0.8	36.2 ± 0.9	160 ± 5	660 ± 17
104 bp	+	S128A	cAMP	298	15.0 ± 0.5	40.9 ± 0.8	69 ± 9	369 ± 30
104 bp	−	S128A	cAMP	298	8.4 ± 0.5	39.5 ± 0.1	57 ± 4	324 ± 13
40 bp	−	S128A	cAMP	296	1.2 ± 0.2	34.5 ± 0.3	160 ± 10	659 ± 34
104 bp	+	CRP*	cAMP	298	9.8 ± 0.1	39.9 ± 0.1	93 ± 11	446 ± 37
104 bp	−	CRP*	cAMP	298	1.6 ± 0.2	35.4 ± 0.3	72 ± 1	360 ± 3
40 bp[a]	−	CRP*	cAMP	296	1.05 ± 0.09	34.1 ± 0.2	120 ± 4	520 ± 14

[a] From ref *4*.

Table 2: Thermodynamic Quantities for the Interaction between the cNMP-Ligated CRP Mutants and Bound RNA Polymerase to the *syncon* Promoter at 298 K

CRP mutant	cNMP	$-\Delta G_b^\circ$ (kJ mol^{-1})	ΔH_b° (kJ mol^{-1})	$T\Delta S_b^\circ$ (kJ mol^{-1})	enhancement of RNA polymerase binding affinity
CRP	cAMP	1.9 ± 0.8	3 ± 4	4.9 ± 4.1	2.1 ± 0.6
T127L	cAMP	2.8 ± 0.7	4.3 ± 0.7	7.1 ± 2.0	3.1 ± 0.8
T127L	cGMP	3.3 ± 0.5	47 ± 8	50 ± 8	3.8 ± 0.8
S128A	cAMP	1.4 ± 0.8	12 ± 9	13 ± 9	1.7 ± 0.1
CRP*	cAMP	4.5 ± 0.3	21 ± 11	26 ± 11	6.1 ± 0.1

Table 3: Thermodynamic Quantities for cAMP-Ligated CRP Mutants Binding to Promoter at 0.5 M KCl Concentration

promoter length (bp)	CRP mutant	cNMP	T (K)	$-\Delta G_b^\circ$ (kJ mol^{-1})	ΔH_b° (kJ mol^{-1})	ΔS_b° (J mol^{-1} K^{-1})
40[a]	CRP	cAMP	296	33.8 ± 0.3	63 ± 2	327 ± 7
104	CRP	cAMP	298	35.1 ± 0.4	62 ± 7	326 ± 23
40[a]	T127L	cAMP	296	27.6 ± 0.4	83 ± 4	351 ± 16
104	T127L	cAMP	298	31.3 ± 0.8	30 ± 7	206 ± 50
40[a]	S128A	cAMP	296	28.7 ± 0.8	75 ± 4	351 ± 16
104	S128A	cAMP	298	31.7 ± 0.3	48 ± 4	267 ± 22

[a] From ref *4*.

of SANS measurements were performed on cAMP-ligated CRP−conDNA, CRP*−conDNA, cAMP-ligated CRP−*syncon* promoter, and cAMP-ligated CRP*−*syncon* promoter complexes in 0, 15, and 70% D_2O/H_2O buffer solutions. The results of the SANS measurements from the cAMP-ligated CRP/mutant−conDNA complexes in these D_2O/H_2O buffer mixtures are presented in Figure 5. As can be seen in Figure 5, the maximum intensities are at 0% D_2O buffer where the intensity is a sum of the intensity contributions from the protein and the DNA components of the complex, while at 70% D_2O, the intensities are at a minimum since the contribution from the DNA component is essentially zero. As shown in Table 4, the *R*g(Complex) values were the same for cAMP-ligated CRP−conDNA and CRP*−conDNA complexes in all the D_2O/H_2O buffer mixtures, even though the scattering from the DNA component is negligible in 70% D_2O buffer and maximum in 0% D_2O buffer. This indicates that a conformational change of the CRP component, rather than the addition of the DNA component, is primarily responsible for the larger-than-predicted *R*g(Complex).

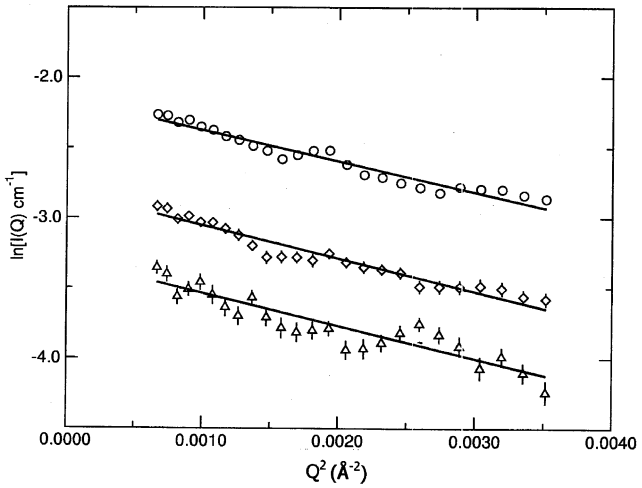

FIGURE 4: Low angle portions of the SANS intensities, on a ln(I) vs Q^2 scale, from the cAMP-ligated CRP−DNA complex in 0% D_2O buffer, measured at concentrations of 2 (○), 1 (◇), and 0.5 mg mL^{-1} (△). Radii of gyration, extracted from the slopes of the fitted curves (—) using a Guinier analysis, were 28.8 ± 1.7, 26.6 ± 0.6, and 26.4 ± 0.8 Å, respectively.

This is further substantiated by decomposition of the SANS contrast variation intensities from the complexes into the $I_{CRP}(Q)$ and $I_{DNA}(Q)$ components of eq 2 as shown in Figure 6a for the cAMP-ligated CRP−conDNA complex and in Figure 6b for the CRP*−conDNA complex. Radii of gyration for the CRP component of the complex were then determined from the distance distribution functions, P(r). The results for the components of the complexes are summarized in Table 5 along with those values expected from the CRP and DNA components in the energy-minimized X-ray crystal structure by Parkinson et al. (*12*). The *R*g(CRP) component in both complexes is ∼28.5 Å, more than 6 Å larger than the 21.6 ± 0.2 Å observed for the cAMP-ligated CRP complex alone (*22*) and the 22.6 Å value predicted from the energy-minimized X-ray crystal structure by Parkinson et al. (*12*). It should be emphasized that the DNA duplex in the crystal structure consists of two staggered 17/14 base sequences annealed together (*12*) and not the continuously linked conDNA duplex employed in this investigation. This may account for the larger *R*g(DNA) in the X-ray crystal structure. The *R*g previously reported (*4*) for the CRP component of the cAMP-ligated CRP−lacDNA was smaller,

Table 4: Radius of Gyration of the DNA-Bound CRP Complex in D_2O/H_2O Buffer Mixtures

CRP complex	DNA	complex concentration in mM (no. of det.)	Radius of Gyration (Å)		
			exp.[a]	X-ray	model
cAMP-ligated CRP	conDNA	0.01−0.04 (5)	27.3 ± 0.8		
in 0% D_2O	conDNA	0.04	28.8 ± 1.7	29.8	30.8
in 15% D_2O	conDNA	0.04	29.9 ± 0.08	28.3	31.9
in 70% D_2O	conDNA	0.04	30.3 ± 1.2	25.5	29.8
cAMP-ligated CRP	lacDNA	0.05−0.90 (2)	31 ± 2		
CRP*	conDNA	0.04−0.06 (3)	28.7 ± 0.6		
in 0% D_2O	conDNA	0.06	28.9 ± 1.0		
in 15% D_2O	conDNA		28.0 ± 1.4		
in 70% D_2O	conDNA		31.3 ± 1.1		
cAMP-ligated T127L	conDNA	0.02(1)	28.8 ± 0.6		
cAMP-ligated CRP	syncon promoter	0.04	55 ± 2		
in 15% D_2O	*syncon* promoter		56 ± 2		
in 70% D_2O	*syncon* promoter		30 ± 3		
cAMP-ligated CRP*	syncon promoter	0.04	53 ± 1		
in 15% D_2O	*syncon* promoter		53 ± 1		
in 70% D_2O	*syncon* promoter		28 ± 2		

[a] Exp. *R*g values were obtained at each concentration using the Guinier approximation, as stated in the text, at only the low *Q* data points from *I*(*Q*) in the region where *QR*g ∼ 1. Those from x-ray were calculated directly from the protein component of the minimized Parkinson et al. X-ray crystal structure (*12*) shown in Figure 7 and those from model were calculated from the minimized distorted structure shown in Figure 7 and described in the text. Except for the T127L + cAMP sample, the stated *R*g value is the average *R*g from all of the separate determinations, and the uncertainty is the standard deviation of that average divided by $n^{1/2}$, where *n* is the number of determinations. The uncertainty for the T127L + cAMP sample was obtained from the statistical uncertainty in the slope of the Guinier approximation equation.

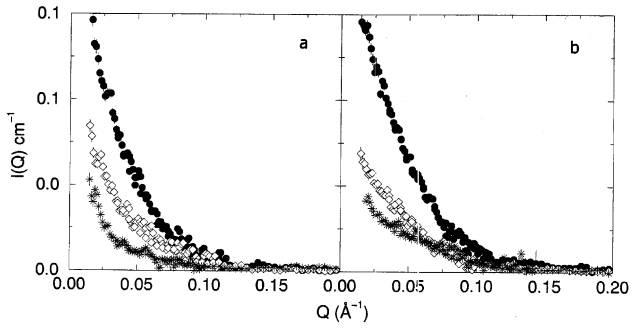

FIGURE 5: Contrast variation SANS intensities from cAMP-ligated CRP−DNA complex (a) and the CRP*−DNA complex (b) in 0 (●), 15 (◇), and 70% D_2O (*) buffers.

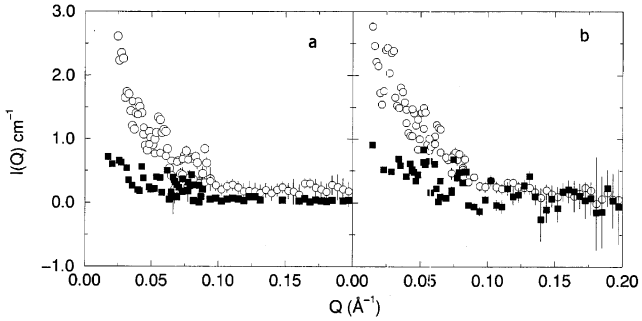

FIGURE 6: Decomposition of SANS contrast variation intensities from the cAMP-ligated CRP−DNA complex (a) and the CRP*−DNA complex (b) into the intensities from the individual components, $I_{CRP}(Q)$ (○) and $I_{DNA}(Q)$ (■), as described in eq 2.

23 ± 1 Å, but was determined without including the data at the lowest *Q* values to minimize what, at the time, were thought to be aggregation effects. This value is also smaller than the previous value (*4*) of 32 ± 1 Å for *R*g(DNA) of the cAMP-ligated CRP−lacDNA complex, which was determined from data obtained at twice the concentration and was influenced by aggregation effects. Now that additional experiments have been performed on three CRP−DNA complexes at lower concentrations, and aggregation effects have been eliminated by verifying that *R*g(Complex) does not change with concentration, it can be concluded that the *R*g value of the CRP component of the complex undergoes an increase upon binding to the DNA. This conclusion is further substantiated by the results from the contrast variation series performed on the cAMP-ligated CRP/mutant−*syncon* promoter complexes shown, in Table 4, a larger *R*g in 0 and 15% D_2O, where the DNA component makes a strong contribution to the scattering intensity. However, the *R*g value in 70% D_2O is approximately the same as the *R*g values for the CRP−conDNA complexes under the same conditions. Upon decomposition of the data into CRP and DNA components, the *R*g value of the CRP and CRP* components were again found to be ∼28 Å, as shown in Table 5.

Model of the CRP Component. To identify the most likely source of the increase in *R*g(CRP), Monte Carlo simulations of the scattering neutron intensities from an energy-minimized distorted conformation of the CRP−DNA complex were generated and compared to the SANS data. A distorted conformation of the X-ray crystal structure of the cAMP-ligated CRP−30 bp DNA complex (*12*) was employed for the starting conformation in the energy-minimization procedure. This distortion was based on the consistent hypersensitivity to several proteases observed in the B α-helix of cAMP-ligated CRP upon DNA binding (*10*). This implies that the conformational change in CRP upon DNA binding involves exposure of this region in the N-terminal domain to the protease. Consistent with this notion, the distortion of the CRP conformation consisted of increasing the torsional angle between the C and B α-helices. The resulting energy-minimized distorted structure is shown in the lower structure in Figure 7. The upper structure in Figure 7 is the energy-minimized closed form of the cAMP-ligated CRP structure without the bound DNA (*7*). Ramachandran plots comparing the protein component of the minimized X-ray crystal structure (*12*), which gives a model SANS intensity similar to the cAMP-ligated CRP structure without the bound DNA (*7*) to the minimized model structure, are presented in Figure 8. The peptide backbones of the CRP

Table 5: Radius of Gyration of the CRP and DNA Components of the Complexes

CRP complex	DNA	complex concentrated (mM)	*Rg*(CRP) (Å)[a]			*Rg*(DNA) (Å)[a]	
			P(*r*)	X-ray	model	P(*r*)	rod model
cAMP-ligated CRP	conDNA	0.04	28.2 ± 0.4	22.9	28.2	26 ± 1	29.1
CRP*	conDNA	0.06	28.7 ± 0.6			27 ± 2	29.1
cAMP-ligated CRP	*syncon*	0.04	28 ± 1	22.9	28.2	53 ± 3	
cAMP-ligated CRP*	syncon	0.04	27 ± 1				

[a] The *R*g values from P(*r*) were obtained from the first moment of the distance distribution function, P(*r*), using all the data points. Those from X-ray were calculated directly from the protein portion of the minimized Parkinson et al. (*12*) X-ray crystal structure shown in Figure 7, and those from the model were calculated from the protein component of the minimized distorted structure shown in Figure 7 and described in the text.

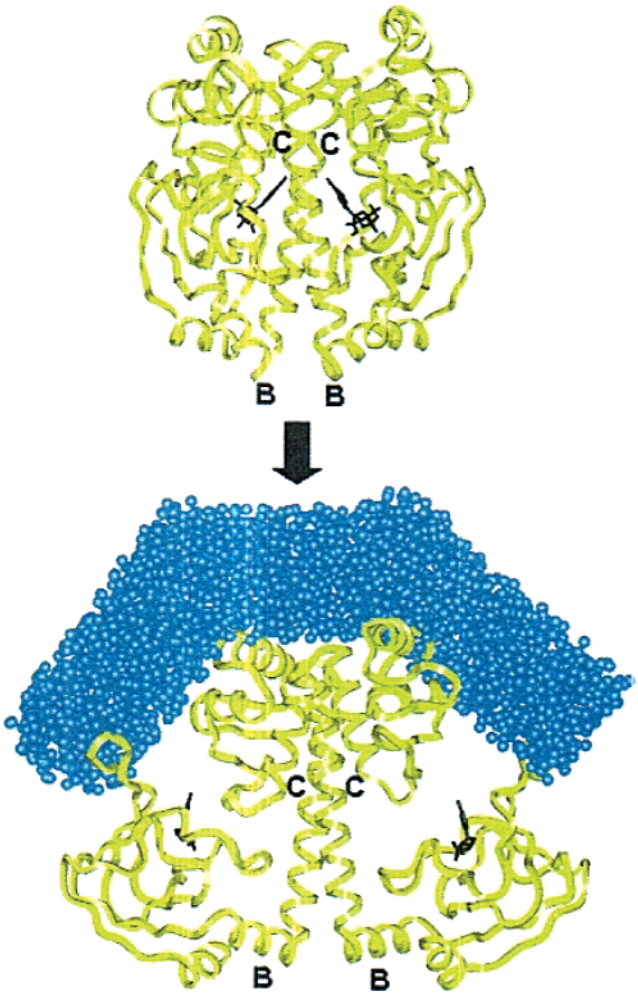

FIGURE 7: Top structure is the energy-minimized structure of cAMP-ligated CRP from Weber and Steitz (*11*) with the cAMP in black. The lower structure is the minimized distorted cAMP-ligated CRP−DNA model structure of Parkinson et al. (*12*) with cAMP (black) added to the binding sites at residues GLU72 and ARG82 only (*13*), which fits the SANS data. The protein component of this model was constructed by increasing the φ angle of residue 108 from −70 to −30° and increasing the ψ angle of residue 18 from 157 to 167°. This distortion resulted in both an opening of the N-terminal domain helices and a slight separation of the C helices. The DNA (blue) is represented by a uniform scattering length density bent rod with a cross-sectional radius of 10 Å.

monomers basically remain intact following alteration of the angle between the B and C α-helices and minimization of the resulting structure. The α-carbon root-mean-square difference between the unminimized and the minimized model structures is 0.001 Å. Distance distribution functions, P(*r*), derived from Monte Carlo simulations of the energy-minimized cAMP-ligated CRP without bound DNA and the protein portion of the distorted cAMP-ligated CRP−DNA structures are compared to the experimental data for the CRP component in Figure 9. The P(*r*) function shown in the figure was derived from the 70% D_2O contrast variation SANS measurement of a 0.04 mM solution of cAMP-ligated CRP complexed with the 40 bp conDNA duplex. These data are identical to the $I_{CRP}(Q)$ data at small *Q* values since the DNA component essentially does not contribute to the scattering intensity in 70% D_2O buffer. However, the higher *Q* data were much noisier for $I_{CRP}(Q)$, and the shoulder at $r \sim 20$ Å in the P(*r*) function could not be resolved for these data. The simulated scattering data provide a closer fit to the experimental data than the simulated scattering data from the energy-minimized structure of the closed form of the cAMP-ligated CRP without the bound DNA (*7*). The shoulder at $r \sim 20$ Å and the peak at $r \sim 45$ Å in the experimental data correspond remarkably well to those obtained from the simulations.

Model of the DNA Component. The bent rod uniform scattering length density model of the DNA is shown in the lower structure of Figure 7. Since the DNA binding site of the protein portion of the distorted energy-minimized structure is not significantly different from that in the undistorted energy-minimized structure of Parkinson (*12*), the latter structure was used to help position the bent rod DNA model in the distorted structure in Figure 7. The distance distribution function, P(*r*), was calculated for the bent rod DNA model and compared to that obtained from the DNA portion of the data from the cAMP-ligated CRP−conDNA complex. As shown in Figure 10, there is a maximum at $r \sim 10$ Å in the model P(*r*) function, but the maximum in P(*r*) obtained from the experimental data occurs at $r \sim 25$ Å. This shift in the P(*r*) maximum can be attributed to an increase in the cross-sectional radius of the DNA duplex in solution. To determine if this can account for the shift in the P(*r*) maximum, the P(*r*) function of a 1:1 mixture of the same bent rods with cross-sectional radii of 10 and 20 Å was simulated and is also shown in Figure 10. Although *R*g(DNA) = 27 Å from this scattering model is still larger than the *R*g = 25 Å value obtained from the data, the distance distribution of this mixed bent rod model fits that of the experimental DNA component data fairly well, and this larger cross-sectional area would be consistent with a slight localized unwinding of about 29° for the promoter upon CRP binding, as reported by Douc-Rasy et al. (*23*) employing an electrophoretic procedure.

SANS measurements on the cAMP-ligated CRP−105 bp *syncon* promoter complex in D_2O/H_2O buffer mixtures exhibited a *R*g of 53 ± 3 Å for the promoter, as shown in Table 5. Using bend rod models for simulating the neutron scattering from the104 bp *syncon* promoter, it was found that the *R*g for the 104 bp DNA duplex bent as shown in

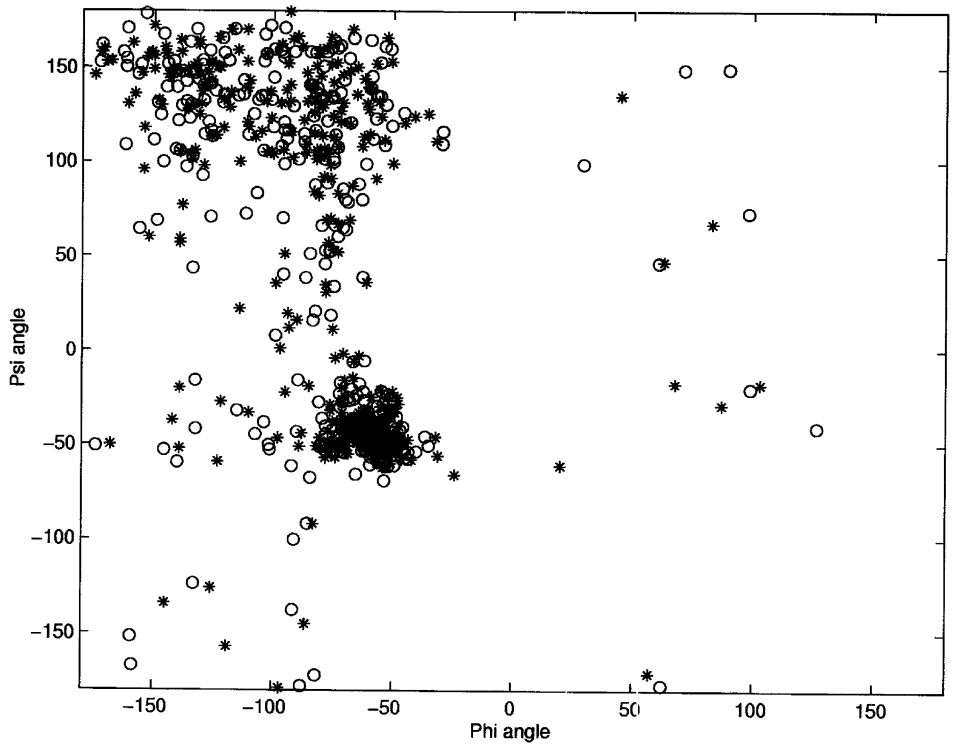

FIGURE 8: Ramachandran plots of the energy minimized cAMP-ligated CRP crystal structure in Figure 7 (*) and the protein component of the energy-minimized cAMP-ligated CRP−DNA model structure shown in Figure 7 (○).

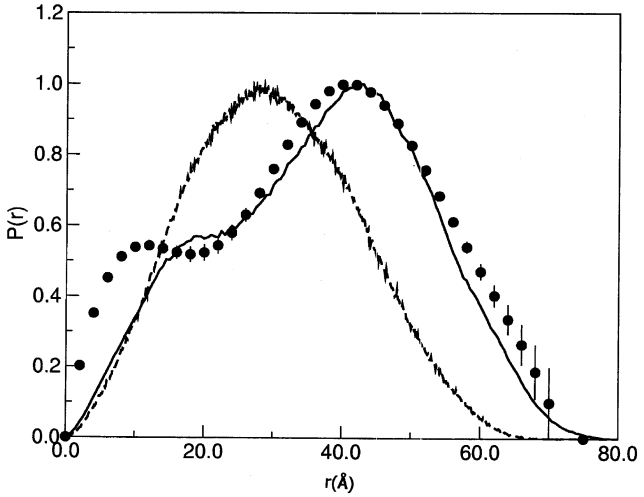

FIGURE 9: Distance distribution function, P(*r*), of the CRP component of the cAMP-ligated CRP−DNA complex derived from the SANS data (●), the minimized Weber and Steitz (*11*) crystal structure (− − −), and the minimized distorted Parkinson et al. (*12*) crystal structure (—). As explained in the text, the experimental P(*r*) was derived from the 70% D_2O contrast variation SANS measurement since the DNA component essentially does not contribute to the scattering intensity under these conditions. The data are identical to the $I_{CRP}(Q)$ data at small *Q* values, yet much less noisy at the higher *Q* values, allowing the shoulder at $r \sim 20$ Å in the P(*r*) function to be resolved.

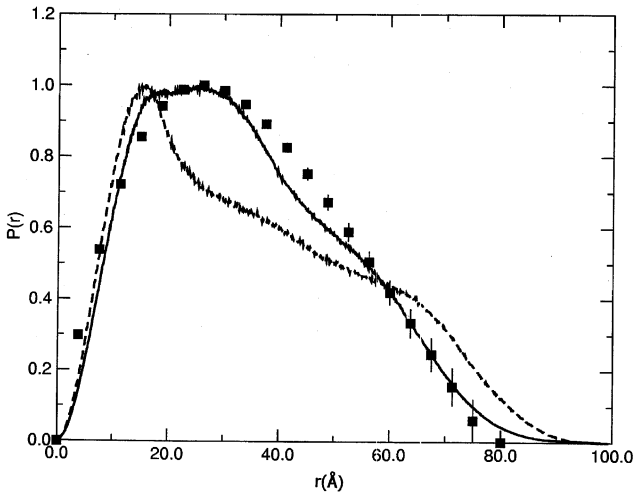

FIGURE 10: Distance distribution function, P(*r*), of the DNA component of the cAMP-ligated CRP−conDNA complex (■). Shown for comparison are the P(*r*) functions for the DNA component calculated from a bent rod with a cross-sectional radius of 10 Å (- - -). The bend angles were obtained from the X-ray crystal structure of Parkinson et al. (*12*). Also shown is the P(*r*) function calculated from a 1:1 mixture of bent rod DNA models with cross-sectional radii of 10 and 20 Å (—).

Figure 7, with the remaining 64 base pairs attached on one side (cane shape) is 69 Å. If the additional 64 base pairs are added symmetrically on each side of the DNA in Figure 7, the calculated *R*g is 48 Å. Since the *R*g value for a straight 104 bp duplex is 103 Å, the experimental results are clearly in better agreement with the bent DNA models. The U-shaped DNA model agrees best, but the *R*g value is a bit smaller (48 Å) than the observed 53 ± 3 Å experimental result, while the cane shaped DNA model gives an *R*g that is too large (69 Å). However, since the long tail portion of the cane was modeled to be straight, it is likely that this tail portion can be bent in such a way as to mimic the *R*g value obtained from experiment. This was not done because, without additional structural data, there are simply too many possible ways to model this additional structural bend.

DISCUSSION

Simulations of the SANS results show that the 104 bp *syncon* promoter is bent by CRP/mutants in an U-shaped

conformation that is partially cane shaped since the *R*g of 53 ± 3 Å is between the calculated *R*g = 48 Å for the exclusive U shape, and the calculated *R*g = 69 Å for the exclusive cane shape bend in solution. Bending of the promoter by CRP/mutant would undoubtedly facilitate the contacts between the CRP/mutants and the RNA polymerase as well as contacts between the promoter and the RNA polymerase. It is unlikely that part of the interaction thermodynamic changes may be attributed to these additional contacts between the promoter and the RNA polymerase since the interaction parameters are different between cAMP-ligated CRP and cAMP-ligated CRP*, while the bend in the promoter remains the same with an *R*g = 53 Å. In addition, simulations of the SANS data on the shorter 40 bp conDNA and lacDNA duplexes bound to CRP/mutants indicate that the DNA duplexes have a larger cross-sectional area than the expected 10 Å diameter for a DNA duplex, which would imply that CRP/mutants induce a partial unwinding of the bound DNA. Since partial unwinding of the DNA is characteristic of the transcriptionally active open form of RNA polymerase, CRP/mutants facilitate the changes associated with isomerization of the RNA polymerase−promoter complex from the closed to the open form.

CRP also increases the binding affinity of the RNA polymerase to the promoter via additional indirect contacts through the bound CRP/mutants. The free energy of this interaction between the CRP and the bound RNA polymerase is entropically driven and ranges from −4.5 to −1.4 kJ mol^{-1} as shown in Table 2. This range is comparable to the estimated free energy range of −5.6 to −3.2 kJ mol^{-1}, determined from gel electrophoresis mobility shift assays, for the interaction between promoter-bound CRP at the −61.5 site and the lac repressor protein bound at a downstream site centered near the transcription start point (*24*). Although the proteins are distally bound, bending of the promoter by the CRP, as observed here in the SANS measurements, would facilitate this interaction. Estimates for a similar interaction between the lac repressor protein and RNA polymerase bound to sites that overlap are, however, higher and range from −12 to −8 kJ mol^{-1} (*24*). This higher range may result from different amino acid residue interactions between the lac repressor protein and the RNA polymerase as well as the closer proximity between the two because of the overlap of their binding sites on the promoter. The interactions between CRP/mutants and the RNA polymerase are entropically driven and exhibit entropy−enthalpy compensation, where changes in the enthalpy are compensated by changes in the entropy. Enthalpy−entropy compensation implies the involvement of water in this interaction. Although there are small endothermic contributions to the interaction enthalpies between RNA polymerase and the CRP/mutants, the overall entropically driven nature of the interaction implies a classical protein−protein hydrophobic interaction. This interaction enhances the binding affinity of the RNA polymerase to the promoter by factors ranging from 1.8 for cAMP-ligated S128A to 6.0 for cAMP-ligated CRP* (Table 2) that contribute to the observed enhancement of transcriptional activation by CRP/mutant. However, this increase can only partially account for the enhancement of transcriptional activation, which ranges from factors of 11−13 (*5*). This further supports the involvement of other mechanisms such as the unwinding of the promoter by CRP/mutants.

The interaction between CRP/mutants and the RNA polymerase may be facilitated by the conformational change in CRP/mutants upon binding to conDNA and lacDNA as evident in the increase in the *R*g of CRP and CRP* from about 22 to 30 Å. This implies that the conformation of the CRP bound to the DNA alone remains the same as when it is bound to the promoter adjacent to the bound RNA polymerase. That this is indeed the case has been demonstrated recently where it was shown that the X-ray crystal structure of CRP in a complex with a 44 bp DNA duplex and the CTD unit of RNA polymerase was superimposable on the structure of CRP bound to the DNA alone (*25*). It should be emphasized that these structures in the crystal state do not necessarily rule out the conformational change observed in the SANS results for CRP in going from the free state to the DNA-bound state in solution. A conformational change resulting from increasing the torsional angle between the C and the B α-helices agrees with the experimental SANS data is shown in Figure 7. In a recent investigation of the X-ray crystal structures of protein−DNA complexes (*26*), it was shown that 11 out of 24 of the systems studied involve rigid domain movements in the protein upon DNA binding, similar to those described here by the distortion in the CRP energy-minimized structure. This distorted CRP structure results in a wider separation between the subunits of promoter-bound CRP, for example, from 8.9 ± 2.5 to 13 Å near the midpoint of the interface at S128, which would allow a closer approach of the proximal CRP subunit to the adjacently bound RNA polymerase. Since residues 156−164 located within the C-terminal domain of the subunit adjacent to the bound RNA polymerase have been implicated as the contacts with RNA polymerase (*1*) and not the residues in the N-terminal domain that becomes more exposed in the distorted structure in Figure 7 (*1*), it is more likely that the wider separation of the subunits in the distorted structure would facilitate contact with the bound RNA polymerase. Since DNA-bound CRP contains both subunits in the closed form, the distortion induced by these mutations may explain why CRP* enhances transcription even without ligation to cAMP as is necessary for the wild-type CRP. The exposure of this region in the N-terminal domain of CRP, however, may directly contribute to the enhancement of transcription of the promoter by CRP bound to a second site centered at −41.5 through its contacts with RNA polymerase. More specifically, a surface loop at K52 in the N-terminal domain of CRP bound at the −41.5 site has been shown to make contact with RNA polymerase (*1*), and the interaction of the K52 loop would be directly affected by the conformational change in CRP shown in Figure 7. However, distortions within CRP that may affect its interaction with RNA polymerase are evident in the CRP* mutant, which exhibits the maximum binding interaction with RNA polymerase in Table 2. A recent X-ray crystal structure of cAMP-ligated CRP* at a resolution of 2.2 Å shows that the interface mutations, T127→L and S128→A on the C α-helix, do indeed introduce some distortion in the CRP as evident by additional bending of the C-terminal domain of one of its subunits, the open subunit, more like the other closed subunit than is observed in the corresponding open subunit of the wild-type cAMP-ligated CRP (*27*).

A comparison of the CRP/mutant binding enthalpies to the *syncon* promoter in the absence of bound RNA polymerase and to conDNA show that the lower endothermic binding enthalpies for the promoter cannot not be attributed to exothermic contributions from additional long-range electrostatic forces on the promoter. The lower binding enthalpy for the longer promoter may be attributed to the energy required for bending of the promoter that is observed in the SANS measurements. The work contribution from bending of the DNA (*28*) is

$$W_{\text{bend}} = 0.5B(\theta^2)/L$$

so that the total enthalpy change upon binding and bending of the DNA is

$$\Delta H_{\text{B}} = W_{\text{bend}} + \Delta H_{\text{I}}$$

where L is the length of DNA undergoing the bending, θ is the angle of the bend, and ΔH_{I} refers to the exothermic enthalpy change resulting from interactions between the amino acid residues on CRP/mutants and the nucleotide bases on the promoter. Since the number of the consensus bases in both the conDNA and the *syncon* promoter that interact with CRP is the same, then ΔH_{I} would be expected to remain the same for both DNA duplexes. However, for the same degree of bending extended over a promoter length of 104 bp, the energy required is only 38% of the energy required for extension of the same bend over the shorter 40 bp conDNA duplex. That this bend is extended over a longer base sequence in the 104 bp *syncon* promoter is evident from the more predominantly U shape of the promoter than the expected cane shape bend that extends over part of the promoter. This would be reflected in a reduction of the endothermic enthalpy required for CRP/mutant binding to the promoter relative to binding to the shorter conDNA, as is indeed observed in Table 1. This difference in the enthalpy would only marginally affect the binding free energy to the promoter since enthalpy−entropy compensation minimizes changes in the binding free energy.

ACKNOWLEDGMENT

S.G. would like to thank the DOE/Sloan foundation for a postdoctoral fellowship in computational molecular biology. B.D.W. is grateful to the Cottrell College Science Program and support through Research Corporation.

REFERENCES

1. Busby, S., and Ebright, R. H. (1999) *J. Mol. Biol. 293*, 199−213.
2. Straney, D. C., Straney, S. B., and Crothers, D. M. (1989) *J. Mol. Biol. 206*, 41−57.
3. Dethiollaz, S., Eichenberger, P., and Geiselmann, J. (1996) *EMBO J. 15*, 5449−5458.
4. Shi, Y., Wang, S., Krueger, S., and Schwarz, F. P. (1999) *J. Biol. Chem. 274*, 6946−6956.
5. Wang, S., Shi, Y., Gorshkova, I., and Schwarz, F. P. (2000) *J. Biol. Chem. 275*, 33457−33463.
6. Schultz, S. C., Shields, G. C., and Steitz, T. A. (1991) *Science 253*, 1001−1007.
7. Petersen, J. M., Skalicky, J. J., Donaldson, L. W., McIntosh, L. P., Alber, T., and Graves, B. J. (1995) *Science 269*, 1866−1869.
8. Patel, L., Abate, C., and Curran T. (1990) *Nature 347*, 572−574.
9. Weiss, M. A, Ellenberger, T., Wobbe, C. R., Lee, J. P., Harrison, S. C., and Struhl, K. (1990) *Nature 347*, 575−578.
10. Baichoo, N., and Heyduk, T. (1998) *J. Mol. Biol. 290*, 37−48.
11. Weber, I. T., and Steitz, T. A. (1987) *J. Mol. Biol. 198*, 311−326.
12. Parkinson, G., Wilson, C., Gunasekera, A., Ebright, Y. W., Ebright, R. E., and Berman, H. M. (1996) *J. Mol. Biol. 260*, 395−408.
13. Passner, J. M., and Steitz, T. A. (1997) *Proc. Natl. Acad. Sci. U.S.A. 94*, 2843−2847.
14. Anderson, W., Schneider, A. B., Emmer, M., Perlman, R., and Pastan, I. (1971) *J. Biol. Chem. 246*, 5926.
15. Lowe, P. A., Hager, D. A., and Burgess, R. R. (1979) *Biochemistry 18*, 1344−1352.
16. Burgess, R. R., and Jendrisak, J. J. (1975) *Biochemistry 14*, 4634−4638.
17. Fried, M. G., and Crothers, D. M. (1984) *J. Mol. Biol. 172*, 241−262.
18. Sambrook, J., Fritsch, E. F., and Maniatis, T. (1989) *Molecular Cloning: A Laboratory Mannual*, 2nd ed., Cold Spring Harbor Laboratory Press, Cold Spring Harbor.
19. Yang, C. P. (1990) *Microcal Data in Origin*, p 66, Microcal Inc., Northhampten, MA.
20. Hammouda, B., Krueger, S., and Glinka, C. J. (1993) *J. Res. Natl. Inst. Stand. Technol. 98*, 31−46.
21. Semenyuk, A. V., and Svergun, D. I. (1991) *J. Appl. Crystallogr. 24*, 537−545.
22. Krueger, S., Gorshkova, I., Brown, J., Hoskins, J., McKenney, K. H., and Schwarz, F. P. (1998) *J. Biol. Chem. 273*, 20001−20006.
23. Douc-Rasy, S., Kolb, A., and Prunell, A. (1989) *Nucleic Acids Res. 17*, 5173−5189.
24. Hudson, J. M., and Fried, M. G. (1990) *J. Mol. Biol. 214*, 381−396.
25. Benoff, B., Yang, H., Lawson, C. L., Parkinson, G., Liu, J., Blatter, E., Ebright, Y. W., Berman, H. M., and Ebright, R. H. (2002) *Science 297*, 1562−1566.
26. Nadassy, K., Wodak, S. J., and Janin, J. (1999) *Biochemistry 38*, 1999−2017.
27. Chu, S., Tordova, M., Gilliland, G. L., Gorshkova, I., Shi, Y., Wang, S., and Schwarz, F. P. (2001) *J. Biol. Chem. 276*, 11230−11236.
28. Bloomfield, V. A., Crothers, D. M., and Tnoco, I., Jr. (2000) *Nucleic Acids, Structures, Properties, and Functions*, p 408, University Science Books, Sausalito, CA.

BI026755V